THE JOURNAL OF PHYSICAL CHEMISTRY C

Article

pubs.acs.org/JPCC

Spectroscopic and Computational Study of Structural Changes in γ-LiV_2O_5 Cathodic Material Induced by Lithium Intercalation

M. B. Smirnov,*[,†] E. M. Roginskii,[‡] V. Yu. Kazimirov,[¶] K. S. Smirnov,[§] R. Baddour-Hadjean,[∥] J. P. Pereira-Ramos,[∥] and V. S. Zhandun[⊥]

[†]Faculty of Physics, St. Petersburg State University, Petrodvorets, 194508 St. Petersburg, Russia

[‡]Ioffe Physical Technical Institute, Polytekhnicheskaya 26, 194021 St. Petersburg, Russia

[¶]Frank Laboratory of Neutron Physics, Joint Institute for Nuclear Research, 141980 Dubna, Russia

[§]Laboratoire de Spectrochimie Infrarouge et Raman, UMR 8516 CNRS − Université de Lille, Sciences et Technologies, 59655 Villeneuve d'Ascq, France

[∥]Institut de Chimie et des Matériaux Paris Est, ICMPE/GESMAT, UMR 7182 CNRS−Université Paris Est-Créteil, 2 rue Henri Dunant, 94320 Thiais, France

[⊥]Kirensky Institute of Physics, Akademgorodok, 660036 Krasnoyarsk, Russia

ABSTRACT: Structure, electronic states, and vibrational dynamics of γ-LiV_2O_5 were studied by combined use of quantum-chemical calculations and Raman spectroscopy. The spin-polarized DFT+U calculations correctly mimic the structural changes induced by the Li intercalation into the V_2O_5 framework. The analysis of the density of electronic states shows that the electrons of Li atoms are transferred to the Vb atoms and are aligned in ferromagnetic order. The charge distribution in the system reflects the change of valence state of the Vb atoms from 5+ to 4+, and it is in line with changes of Vb−O bond lengths. The calculated Raman spectrum of the γ-LiV_2O_5 structure is in line with the experimental Raman spectra that allows a reliable assignment of all prominent Raman peaks. Comparison of the spectra of γ-LiV_2O_5 and γ'-V_2O_5 indicates spectral signatures of structural changes induced by the Li insertion into the γ'-V_2O_5 lattice. Results of the study present the opportunity of using Raman spectroscopy for characterization of structural modifications of the vanadate framework upon intercalation of guest species.

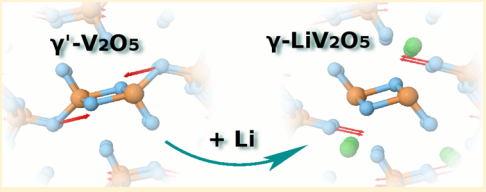

INTRODUCTION

Vanadium pentoxide has been widely studied as cathode active material in rechargeable lithium batteries due its ability to accommodate lithium ions,[1] and this system continues to attract much interest due to the existence of many lithiated $Li_xV_2O_5$ phases occurring during the electrochemical reaction $V_2O_5 + xLi^+ + xe^- \leftrightarrow Li_xV_2O_5$. In fact, ternary Li−V−O oxides can adopt various crystal modifications depending on the lithium content and formation temperature.[2] The phase predominance diagram for this system at room temperature has been described previously,[3,4] and the diagram shows three single-phase regions: α-$Li_xV_2O_5$ for $0 < x < 0.13$, ε-$Li_xV_2O_5$ for $0.32 < x < 0.8$, and δ-$Li_xV_2O_5$ for $0.88 < x < 1.00$. These low-temperature phases appear to be structurally very similar to the α-V_2O_5 polymorph. At higher lithium content and at temperatures >400 °C, a major rearrangement of the V_2O_5 framework occurs, and the γ-LiV_2O_5 crystal modification is formed.[5] A pronounced puckering of the V_2O_5 layered framework accompanied by breaking of some V−O bonds has been described for this phase.[6]

From an electrochemical point of view the voltage composition curve of V_2O_5 was found to be in accord with this $Li_xV_2O_5$ phase diagram.[4,7−9] Indeed, several structural transformations of the bulk material take place depending on the amount of Li ions x intercalated in the V_2O_5 pristine structure. The α-, ε-, and δ-$Li_xV_2O_5$ phases were identified in the $0 < x \leq 1$ composition range, and a reversibility of the Li insertion was established; that is, the structure of the parent α-V_2O_5 polymorph can be recovered upon deintercalation. Conversely, if more than one lithium ion per structural unit is accommodated, irreversible structural changes resulting in the formation of the γ-LiV_2O_5 phase take place.[7−9] The layered structure of γ-LiV_2O_5 with a mixed V^{5+}/V^{4+} valence state of the metal ions, together with a relatively high lithium content, makes this phase very interesting as cathode material for lithium-ion batteries.[10−14] In such batteries using carbon as the anode material, the cathode active material must be in fully lithiated state, thus allowing Li^+ ions to be produced through the oxidation of the positive electrode during the first charge. The electrochemical and chemical oxidations of the γ-LiV_2O_5 phase accompanied by the Li ion deintercalation were reported to lead to a new metastable γ'-form of V_2O_5[8,9] that keeps the memory on the structure of the original lithiated phase.[9] The understanding of the Li intercalation process at the atomic level

Received: June 10, 2015
Revised: August 24, 2015
Published: August 25, 2015

DOI: 10.1021/acs.jpcc.5b05540
J. Phys. Chem. C 2015, 119, 20801−20809

and of its consequence for the geometric and electronic structure of the γ'-V_2O_5/γ-LiV_2O_5 materials is, therefore, of utmost importance for their potential applications. However, only a few studies have been devoted to this topic.[13,15]

Calculations based on the density functional theory (DFT) were used to study the electronic structures of γ'-V_2O_5[10,11] and γ-LiV_2O_5[12] and to model the impact of Li intercalation on the electronic states.[13] The bottom states of the conduction band in the systems were obtained to be formed by 3*d* states of V atoms.[10,12] Calculations showed that the intercalation of Li atoms into the structure resulted in the appearance of states in the gap that were due to the transfer of 2*s* electrons of Li to the *d* states of vanadiums.[12,13] Both the appearance of the gap state and its position were found to be in line with the experimental data by photoelectron spectroscopy.[16] These computational studies, however, did not concern the vibrational dynamics of these structures, although the methods of vibrational spectroscopy and Raman spectroscopy, in particular, have been proved to be a powerful and sensitive tool for studying structural and bonding changes occurring in oxide materials at structural phase transitions.[14]

The present work reports results of a combined experimental and computational study of the structure, charge distribution, and vibrational dynamics of the γ-LiV_2O_5 material. The γ-LiV_2O_5 sample was synthesized through a carbothermal reduction method and was characterized by means of X-ray diffraction (XRD) measurements and Raman spectroscopy. The analysis of the experimental data was assisted by results of DFT computations of the structure and vibrational states of the γ-LiV_2O_5 lattice with a particular emphasis on the Raman-active vibrational modes. This analysis relies on the outcome of our recent study on the structure and vibrational dynamics of γ'-V_2O_5 obtained by the delithiation of the γ-LiV_2O_5 material.[17] Comparison of the experimental and computational results allows us to propose a complete assignment of peaks in the Raman spectra to vibrations of particular structural units. A Raman feature pointing to the intercalation of Li ions into the γ'-V_2O_5 framework was identified. The work highlights the efficiency of the combined approach as a powerful tool for understanding the structural changes induced by Li insertion into the γ'-V_2O_5 lattice at the atomic level.

EXPERIMENTAL DETAILS

γ-LiV_2O_5 powder was synthesized through the carbothermal reduction (CTR) method described in ref 18. The method consists of mixing carbon, Li, and V precursors and then subjecting the mixture to a thermal treatment. Carbon black (Alfa Aesar), α-V_2O_5 (Merck), and lithium carbonate (Alfa Aesar) were used as the precursors, and the CTR reaction can be written as

$$0.5Li_2CO_3 + V_2O_5 + 0.25C \rightarrow \gamma\text{-}LiV_2O_5 + 0.75CO_2$$

Precise CTR conditions are required to obtain the pure γ-LiV_2O_5 material. The ratio of the concentrations $[V_2O_5]/[Li]$ was taken equal to 1, and 25% mass excess of carbon was used over the stoichiometric CTR reaction. The precursors were initially intimately mixed and then pelletized using a hydraulic press. The pellet was then heated at 600 °C in an N_2 atmosphere during 1 h using a 5 °C/min heating rate. The XRD experiments were performed using a Panalytical XPert pro apparatus equipped with an X'Celerator detector and using Co Kα radiation ($\lambda_{K\alpha}$ = 1.789 Å). The Rietveld refinements were performed with GSAS software.[19,20]

The Raman spectra in the VH polarization were recorded at room temperature using a micro-Raman system with a Labram HR800 spectrometer equipped with a charge-coupled device (CCD) detector. A He−Ne laser (633 nm) was used as the excitation source. The spectra were measured in the back-scattering geometry with the resolution of about 0.5 cm^{-1}. A 100× objective was used to focus the laser beam to a spot of 1 μm^2 size on the sample surface, and the laser power was fixed at 0.2 mW to avoid any degradation of the sample.

COMPUTATIONAL DETAILS

The calculations were carried out with VASP code[21,22] using the plane-wave basis set for valence electronic states. Exchange and correlation were treated within the GGA approximation to DFT with the Perdew−Burke−Ernzerhof (PBE) exchange-correlation functional.[23] The projector-augmented wave (PAW) method[24,25] was used to describe the interactions between the core and valence electrons. The 3*p*3*d*4*s* states of the V atom and 2*s*2*p* states of the O atom were considered as valence states, whereas the Li atom was treated at the all-electron level. All calculations were fully spin polarized (SP) to account for the reduction of the transition metal oxide structure upon Li intercalation into the framework. The DFT+U scheme by Dudarev et al.[26] was employed to take the localization of vanadium 3*d* states into account. The value of *U* equal to 4 eV was determined previously by Scanlon et al.[13] A proper modeling of interlayer distances in the layered V_2O_5 framework was shown to necessitate the consideration of dispersion interactions.[27,28] These interactions were taken into account with the semiempirical D2 correction.[29]

To calculate the equilibrium lattice parameters, optimizations of γ-LiV_2O_5 structure were performed for a series of five volumes of unit cell. In each case, the atomic positions and cell parameters were allowed to relax, whereas the volume and the symmetry of the lattice were kept fixed. The structural optimization was deemed to be converged when the maximum force on ions was $<2 \times 10^{-3}$ eV $Å^{-1}$. The resulting energy versus volume curve was fitted by the Murnaghan equation of state[30] to obtain the equilibrium cell volume. This approach avoided the problems related to the Pulay stress and the changes of the plane-wave basis set size that accompany volume variations.

The results were checked for convergence with respect to *k*-point sampling and plane-waves kinetic energy cutoff. It was found that convergence of total energy within 2.5 meV was achieved with the energy cutoff of 950 eV and with a $2 \times 6 \times 2$ grid of *k*-points chosen according to the Monkhorst−Pack scheme[31] in the irreducible part of the Brillouin zone. The minimum energy lattice parameters thus determined were employed in all subsequent calculations that were performed using the same calculation parameters and with the same convergence criterion. The phonon spectrum in the Γ point of the Brillouin zone was computed using the density functional perturbation theory (DFPT) approach.[21,22]

The complete Raman spectrum of the γ-LiV_2O_5 material was obtained by computation of the Raman scattering intensities of Raman-active vibrational modes. The intensity I_k^{VH} of mode *k* in the theoretical VH spectrum of powder sample was obtained as

$$I_k^{VH} = \frac{(\omega_0 - \omega_k)^4}{\omega_k(1 - \exp(-\hbar\omega_k/k_BT))} R_k^{VH} \quad (1)$$

DOI: 10.1021/acs.jpcc.5b05540
J. Phys. Chem. C 2015, 119, 20801−20809

where ω_0 is the frequency of the incident radiation, T is the temperature, and $\hbar$ and k_B have their conventional meanings. The quantity R_k^{VH} in eq 1 is the VH Raman activity of mode k

$$R_k^{VH} = [(A_{xx} - A_{yy})^2 + (A_{yy} - A_{zz})^2 + (A_{zz} - A_{xx})^2 + 6(A_{xy}^2 + A_{xz}^2 + A_{yz}^2)]/30 \quad (2)$$

with $A_{\alpha\beta}$ (α,β = x,y,z) being the Cartesian components of Raman tensor $\mathbf{A}_k$. R_k^{VH} is computed using the assumption of linearly polarized incident radiation.

The tensor $\mathbf{A}_k$ of the vibrational mode k is related to the derivative of the macroscopic dielectric tensor $\boldsymbol{\epsilon}$ with respect to the normal vibrational coordinate Q_k as

$$\mathbf{A}_k = \frac{\sqrt{\Omega}}{4\pi}\frac{\partial \boldsymbol{\epsilon}}{\partial Q_k} \quad (3)$$

with Ω being the unit cell volume. As VASP does not provide the possibility of computing the Raman tensor within DFPT, the components of $\mathbf{A}_k$ tensors were obtained by the numerical differentiation of $\boldsymbol{\epsilon}$. The dielectric tensor was calculated as the frequency-dependent dielectric matrix.[32] The calculations of the matrix were carried out for the two frequency values below ω = 241.8 THz (1 eV) and above ω = 604.5 THz (2.5 eV), respectively, the band gap value (ca. 1.6 eV) of γ-LiV_2O_5. The Cartesian displacements of atoms in the vibrational modes were derived from the corresponding eigenvectors of the mass-weighted Hessian matrix. The displacement amplitude of vibrational modes Q_k was equal to 0.25 Å (amu)$^{1/2}$.

For comparison with the exprimental spectrum, the resulting Raman stick spectrum was convoluted with a Lorentzian function with HWHM = 4 cm^{-1}.

RESULTS AND DISCUSSION

Structure of γ-LiV_2O_5. The measured XRD pattern of the γ-LiV_2O_5 material is shown in Figure 1, which also compares it with a pattern simulated using the structural data reported by Galy et al.[5] The excellent agreement of the measured and simulated patterns unambiguously indicates that the synthesized material is indeed γ-LiV_2O_5. The peaks in the experimental pattern can be indexed on the basis of orthorhombic symmetry (*Pnma* or D_{2h}^{16} space group). The refinement of the data has resulted in the unit cell parameters a = 9.694, b = 3.607, and c = 10.685 Å, which are very close to those previously reported in refs 5 and 9. Unfortunately, a small amount of the Li_3VO_4 phase present in the sample did not allow us to reliably determine fractional coordinates of atoms. Consequently, in what follows, the experimental structure by Galy et al.[5] is used for comparison with results of the DFT calculations.

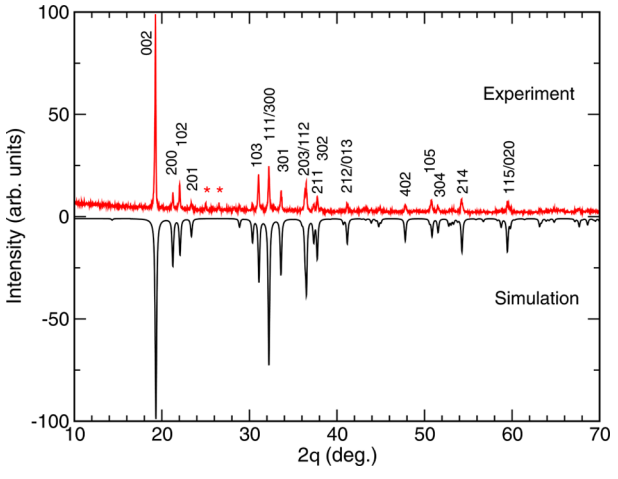

Figure 1. Comparison of experimental (present work) and simulated XRD patterns of γ-LiV_2O_5 material. The simulated pattern was computed using the experimental structure of ref 5, and the intensities were taken negative for the sake of comparison. Asterisks in the experimental pattern denote peaks due to traces of Li_3VO_4 phase in the sample.

Similarly to the lattice of the α-V_2O_5 polymorph (the ground state structure of divanadium pentoxide), the γ-LiV_2O_5 lattice consists of layers stacked perpendicularly to the z-axis (Figure 2, panels a and b, respectively). In both structures the layers are

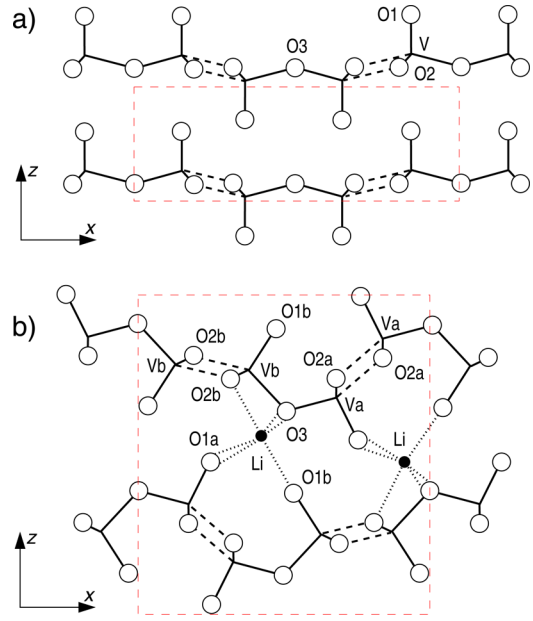

Figure 2. Structures of α-V_2O_5 (a) and γ-LiV_2O_5 (b) lattices in the projection along the b-crystallographic direction (y-axis). V−O interchain contacts (ladder steps) are shown by dashed lines; the Li−O bonds are depicted by dotted lines; red dashed rectangles indicate the unit cells of the structures.

built of infinite V_2O_5 chains shown by solid lines in Figure 2. The chains run in the y-direction and are interconnected by the V−O linkages that are often viewed as "ladder steps" (LS) depicted in Figure 2 by dashed lines. The intercalated Li atoms form six Li−O bonds connecting each Li atom with three vanadyl atoms (O1a and O1b) of one layer and with three bridging oxygen atoms (O2b and O3) of another layer (Figure 2b). The authors of refs 5 and 9 suggested that the γ-LiV_2O_5 and γ'-V_2O_5 lattices are isostructural. According to this suggestion, the Li atoms occupy octahedral sites in the interlayer space of the γ-LiV_2O_5 lattice and their presence in the void does not induce a significant distortion of the vanadium oxide framework.

Table 1 provides the lattice parameters and fractional coordinates of atoms of γ-LiV_2O_5 obtained in the DFT calculations and compares them with the experimental data.[5] One can see that the DFT calculations well reproduce the experimentally determined lattice characteristics with a maximum deviation of 1.1% for the c-lattice parameter. Note that the framework layers in the structure are stacked along the

DOI: 10.1021/acs.jpcc.5b05540
J. Phys. Chem. C 2015, 119, 20801−20809

Table 1. Lattice Parameters (in Å) and Fractional Coordinates of Atoms in the γ-LiV_2O_5 Structure (*Pnma* Space Group, No. 62) Obtained in the DFT Calculations in Comparison with the Experimental Data[5]

	DFT, present work			experimental[5]		
a,*b*,*c*:	9.7908	3.6013	10.7808	9.702	3.607	10.664
	x	*y*	*z*	*x*	*y*	*z*
Vb	0.1265	0.2500	0.9992	0.1238	0.2500	0.9991
Va	0.4325	0.2500	0.1022	0.4339	0.2500	0.0995
O3	0.2594	0.2500	0.1412	0.2590	0.2500	0.1330
O1a	0.0208	0.2500	0.2681	0.0170	0.2500	0.2700
O1b	0.2325	0.2500	0.8791	0.2180	0.2500	0.8760
O2b	0.4297	0.2500	0.5529	0.4260	0.2500	0.5490
O2a	0.0601	0.2500	0.5457	0.0600	0.2500	0.5460
Li	0.3416	0.2500	0.7268	0.3370	0.2500	0.7750

c-axis and the size of the cell in this direction is largely determined by the dispersion interactions. Our preliminary calculations without the D2 correction, at the PBE_SP+U level, have resulted in a difference of 3.3% for the *c*-lattice parameter. The difference is significantly smaller than the overestimations of 11 and 7% obtained at the same level of theory for the α-V_2O_5 structure by Londero and Schröder[27] and by Carrasco,[28] respectively. A better agreement of the *c*-parameter with the experimental data in the case of the calculations of the lithiated structure might be explained by the interaction of Li atoms with the V_2O_5 framework that strengthens interlayer interactions, thus reducing the importance of the dispersion correction for the interlayer spacing.

Table 2 compares interatomic distances in γ-LiV_2O_5 and γ'-V_2O_5 structures computed in the present work with the experimental data of refs 5 and 9, respectively. In both structures the calculated V−O bond lengths agree with their experimental counterparts with the relative root mean squared error (RRMSE) of 2.9% (maximum RRMSE of 5.6%). Despite a slight systematic overestimation of the interatomic distances due to the use of the PBE exchange-correlation functional, one can conclude that the geometry of the V_2O_5 layers is well mimicked by the calculations.

Analyzing the experimental structural characteristics of γ'-V_2O_5 and γ-LiV_2O_5 lattices (Table 2), one can distinguish structural changes induced by the lithium intercalation. They can be summarized as follows: (i) the unit cell shortens in the *a*-direction and lengthens in the *c*-direction with a negligible change in the *b*-direction; (ii) the length of the vanadyl V−O1 bonds increases; (iii) the Va−O3−Vb bridge becomes markedly asymmetric with a lengthened Vb−O3 bond and a shortened Va−O3 one. In addition, the presence of Li atoms in the structure modifies the length of Vb−O2b bonds, whereas the Va−O2a bond length remains almost unchanged. This fact can be related to the formation of the Li−O2b bonds; note that the O2a atoms do not form bonds with Li atoms. All of these changes are nicely reproduced by the DFT calculations, and the differences between the two structures will later be used while discussing the vibrational spectra of the two materials.

Electronic Structure and Charge Distribution. Figure 3 shows the density of states (DOS) for γ-LiV_2O_5 computed in

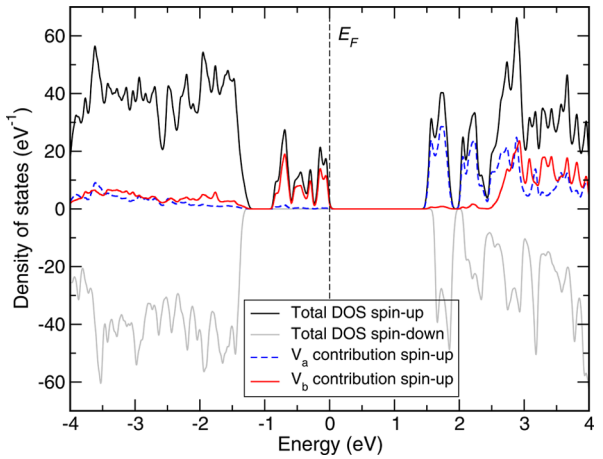

Figure 3. Density of states for γ-LiV_2O_5 structure with the DOS for the spin-up and spin-down electron states shown above and below the abscissa axis, respectively. Contribution to the spin-up DOS from the Va and Vb atoms are shown by dashed blue and solid red lines, respectively.

Table 2. Experimental and Calculated Unit Cell Parameters and Bonds Lengths (in Å) in γ'-V_2O_5 and γ-LiV_2O_5

	experimental		calculated	
	γ'-V_2O_5[9]	γ-LiV_2O_5[5]	γ'-V_2O_5	γ-LiV_2O_5
a	9.9461	9.702	10.1346	9.7908
b	3.5852	3.607	3.6163	3.6013
c	10.0423	10.664	10.1931	10.7808
Vb−O1b	1.5482	1.5995	1.6057	1.6593
Vb−O3	1.7257	1.9389	1.8220	2.0096
Vb−O2b	2 × 1.8919	2 × 1.9414	2 × 1.9062	2 × 1.9699
$(Vb-O2b)_{LS}$	1.9855	1.9864	2.0396	2.0067
Va−O1a	1.5824	1.6083	1.6087	1.6436
Va−O3	1.8467	1.7341	1.8009	1.7462
Va−O2a	2 × 1.8962	2 × 1.8925	2 × 1.9165	2 × 1.9022
$(Va-O2a)_{LS}$	1.9715	1.9759	2.0158	2.0259
Li−O1b		1.9814		1.9588
Li−O2b		2.0660		2.0639
Li−O3		2 × 2.2545		2 × 2.2519
Li−O1a		2 × 2.3429		2 × 2.2927

DOI: 10.1021/acs.jpcc.5b05540
J. Phys. Chem. C 2015, 119, 20801−20809

the present work. States up to ∼0.9 eV below the Fermi level (E_F) correspond to the gap states observed experimentally[16] and found in previous calculations.[12,13] These states are the *d* states of vanadium atoms occupied by the 2*s* electrons of Li atoms. The computation of the partial DOS reveals that only states due to the Vb atoms are filled, as illustrated in Figure 3, whereas the states of the Va atoms remain virtually empty. Furthermore, Figure 3 shows that the electrons occupy exclusively spin-up states, thus resulting in ferromagnetic order with spins of four electrons per unit cell aligned. Bader analysis[33] of the spin-projected electron density points to different spin occupations on the Va and Vb atoms: 4.3727 and 4.3208 e^- with spin-up and spin-down on the former, and 4.9864 and 3.9426 e^- with spin-up and spin-down on the latter atom.

The existence of the gap state was observed by UV photoelectron spectroscopy.[16] According to these experimental data, the gap state at ∼1.3 eV above the valence band is due to the occupation of V3*d* states by electrons from the 2*s* states of Li atoms. A computational study of γ-LiV_2O_5 by Valenti et al.[12] revealed that the four lowest-lying 3*d* bands at the Fermi level have a dominant contribution from the Vb atoms and are half-filled. Scanlon et al.[13] in their modeling study of Li-intercalated V_2O_5 structures found a new localized state at ca. 0.9 eV above the valence band upon insertion of the Li atom in the interlayer space. For the γ-LiV_2O_5 structure the authors obtained the presence of a double peak in the band gap, ca. 0.8 eV above the valence band. The results of the present study are in perfect agreement with these findings.

Table 3 reports atomic charges obtained by the Bader analysis of the electron density in γ-LiV_2O_5 and γ'-V_2O_5, with the last column giving the change of atomic charge upon Li intercalation. The charge of the Li atom is close to the formal ionic charge of the Li cation that indicates an almost complete loss of the 2*s* electron by the atom. The ejected electron is shared by almost all atoms of the vanadate framework, although to different extents. One sees that the Vb and O1b atoms accept >50% of the negative charge, whereas the charges of the Va and O2a atoms vary in minimum degree.

Table 3. Bader AIM Charges (in au) of Atoms in the Structures of γ-LiV_2O_5 and γ'-V_2O_5

atom	γ-LiV_2O_5	γ'-V_2O_5	ΔQ
Va	2.3065	2.3452	−0.0387
Vb	2.0710	2.3396	−0.2686
O1a	−0.8875	−0.7410	−0.1465
O1b	−0.9586	−0.7084	−0.2502
O2a	−1.1418	−1.1424	0.0006
O2b	−1.2303	−1.1258	−0.1045
O3	−1.0545	−0.9674	−0.0871
Li	0.8951		0.8951

The charge fraction transferred from Li atoms to a particular O atom is related to the length of the corresponding Li−O bond (cf. Table 2). Thus, the most significant charge transfer occurs along the Li−O1b and Li−O2b bonds, which are the shortest ones. A notable charge increment on O1a atoms can be related to formation of two Li−O1a bonds (ΔQ = 0.0733 e^- per bond). The only exception of this trend is a small charge variation on the O3 atom, which forms two Li−O3 bonds of intermediate length. This pecularity might be due to the fact that the gain of electron density from Li atoms is partially leveled by density loss caused by the lengthening Vb−O3 bond in the γ-LiV_2O_5 structure (Table 2). Note that the O2a atoms do not form bonds with the Li atoms and, consequently, their charge is not altered by the Li intercalation.

A direct Li to V charge transfer is highly improbable because of the significant distance between the atoms. One can rather assume that the electron density is transferred to the V atoms via the oxygen atoms forming Li−O bonds. Table 3 shows a large difference in the charge variation on Va and Vb atoms upon Li intercalation. In line with the analysis of the DOS, the Vb atom accepts by an order of magnitude more electron density than the Va atom. It is noteworthy that the amount of negative charge transferred to the Vb atom (∼0.27 e^-) is in good agreement with the value of 0.32 e^- obtained from the analysis of the XPS data.[16] Such a significant charge variation on the Vb atom reflects the V^{5+} to V^{4+} change of the valence state.[16] Hence, the lengthening of all Vb−O regular bonds (except the ladder step Vb−O2b contacts) seen in Table 2 upon Li intercalation can be interpreted as a result of the valence state change of the vanadium atoms.

Raman Spectrum of γ-LiV_2O_5 Material. The experimental Raman spectrum of the γ-LiV_2O_5 powder sample obtained in the present work via the CTR method is displayed in Figure 4, and the positions of peaks in the spectrum are listed in Table 4. The spectrum can be compared with results of two previous works dealing with the Raman spectra of the γ-LiV_2O_5 material.[34,35] The study by Popovic et al.[34] reported polarized Raman spectra of a single-crystal γ-LiV_2O_5 sample with the spectra recorded in different polarization settings and at different temperatures. The second study[35] was devoted to the Raman spectroscopic characterization of $Li_xV_2O_5$ structures and, in particular, of the γ-LiV_2O_5 phase obtained via thermal treatment of δ-LiV_2O_5. Data of the former work, being more complete, are used for comparison with the results of the present study.

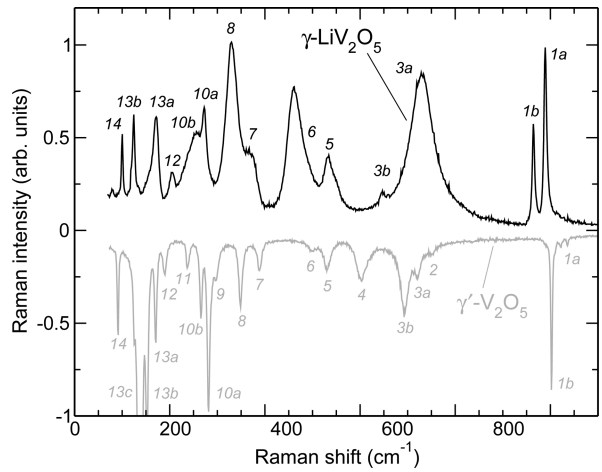

Figure 4. Raman spectra of γ-LiV_2O_5 and of γ'-V_2O_5.[17] The Raman intensity in the γ'-V_2O_5 spectrum was taken negative for the sake of clarity. The vibrational peaks in the spectra due to the vibrational modes of the same origin are labeled by the same numbers (see also Table 2 in ref 17).

Comparison of the spectrum in Figure 4 with those reported in ref 34 shows that all spectral peaks present in the spectrum of powder exist in the spectra of a single crystal. The difference between the positions of observed peaks in the two sets of spectra does not exceed 6 cm^{-1}. The most notable distinction

DOI: 10.1021/acs.jpcc.5b05540
J. Phys. Chem. C 2015, 119, 20801−20809

Table 4. Position of Peaks (in cm^{-1}) in the Experimental Raman Spectrum of γ-LiV_2O_5 (Figure 4) and Calculated Wavenumbers of Raman-Active Vibrational Modes

		calculated				
peak[a]	experimental	A_g	B_{2g}	B_{1g}	B_{3g}	assignment
1a	987	975	1015			ν(Va−O1a) + ν(Vb−O1b)
1b	965	963	962			ν(Va−O1a) + ν(Vb−O1b)
		793	819			ν(Va−O3)
3a	737			736	736	ν_{as}(Va−O2a−Va)
3b	646			628	628	ν_{as}(Vb−O2b−Vb)
5	549	532	521			ν(Va−O2a)$_{LS}$
6	533	515	514			ν(Vb−O2b)$_{LS}$
		484	537			ν(Vb−O3) + LM(a,b) (Va,Vb)
	462					
		409	449			Li + LM(a,c) (Vb)
7	369	376	376			Li + LM(a,c) (Vb)
		355	344			Li + LM(a,c) (Va,Vb)
8	329	332	332	338	335	Li + LM(a,c) (Va,Vb), LM(e) (Vb) + O3(y)
				294	300	Li(y) + O1a(−y)
10a	272	286	295	277	277	Li(x) + LM(a,c) (Va), Li(y) + LM(e) (Va)
10b	253	255	272			Li + LM(c,d) (Va)
				235	230	Li(y) + O3(y)
12	205	209	220			LM(d) (Va,Vb)
13a	171	171	192	172	178	LM(c,d) (Va,Vb), LM(f) (Va)
				159	156	LM(f) (Vb)
13b	124	127	158			Rot(y) (Va)
14	100	96	140			Rot(y) (Vb)

[a]The peak numbers correspond to those in Figure 4.

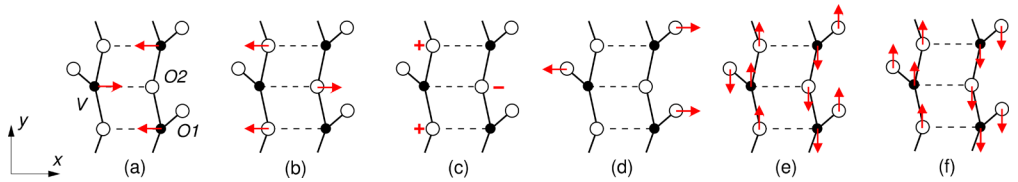

Figure 5. Distortions of the V_2O_5 framework ladders contributing to the Raman-active vibrational modes: (a−d) to the A_g and B_{2g} modes; (e, f) to the B_{1g} and B_{3g} modes.

between the powder and single-crystal spectra concerns the width and relative intensities of some peaks. These differences can be explained by the inhomogeneous size and random orientation of microcrystallites in the powder γ-LiV_2O_5 material that affect the relative Raman intensities and result in peak broadening. Furthermore, some of the single-crystal spectra in ref 34 were measured at a temperature of 10 K and, therefore, the peak width in these spectra is essentially smaller than in the powder spectra recorded at room temperature.

The following discussion of the γ-LiV_2O_5 Raman spectrum makes use of our results on the analysis of the vibrational dynamics of the γ'-V_2O_5 lattice.[17] According to this analysis, the vibrational spectrum of the layered V_2O_5 structure can be interpreted with the help of a twin-mode scheme. The scheme implies that the inphase and antiphase combinations of the analogous vibrational modes localized in neighboring layers have close vibrational frequencies because of the weakness of interlayer interactions. The vibrational modes of the γ-LiV_2O_5 structure in the Γ-point of the Brillouin zone are distributed over irreducible symmetry representations as

$$\Gamma = 16A_g + 16B_{2g} + 8B_{1g} + 8B_{3g} + 8A_u + 8B_{2u} + 16B_{1u} + 16B_{3u}$$

with g and u modes being active in Raman and infrared spectra, respectively. The twin-mode scheme then suggests that the A_g and B_{2g} symmetry species contain twin modes corresponding to the inphase and antiphase atomic oscillations in the xz plane, respectively, whereas the B_{1g} and B_{3g} species consist of twin modes with the inphase and antiphase atomic oscillations in the y-direction, respectively. Furthermore, the antiphase B_{2g} and B_{3g} combinations are expected to have lower Raman intensities than the inphase ones because of a cancellation effect.

The calculated frequency values of the Raman-active vibrational modes of the γ-LiV_2O_5 structure are gathered in Table 4, and the mode assignment based on the analysis of the amplitudes of atomic displacements is given in the last column. Specifying the assignment we use the following notations: ν, bond-stretching mode; LM(X) (Y), ladder mode, where X is the type of distortion shown in Figure 5 and Y is the type of V atom in the ladder; Rot(y), rotation of the ladders around the y-axis; X(y), mode with the maximum amplitude of the atoms X in the y-direction. The computational data in Table 4 show that the frequencies of the modes are in line with the behavior predicted by the twin-mode scheme. This is particularly true for the B_{1g} and B_{3g} modes, for which the frequency difference does not exceed a few wavenumbers.

If the γ-LiV_2O_5 and γ'-V_2O_5 materials were isostructural, their Raman spectra would be similar to the only distinction as the appearance of new peaks related to the vibrational modes of

DOI: 10.1021/acs.jpcc.5b05540
J. Phys. Chem. C 2015, 119, 20801−20809

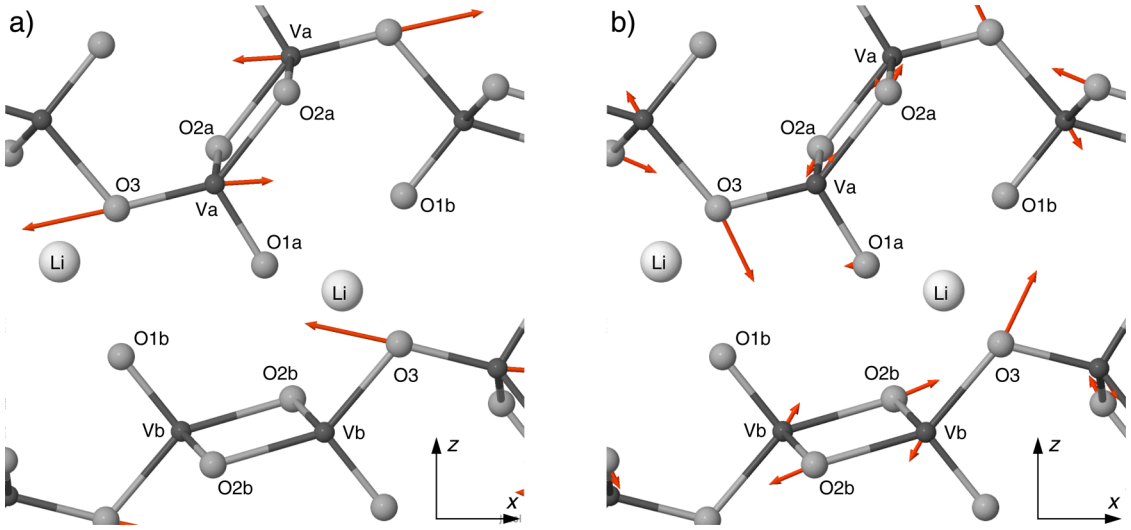

Figure 6. Displacements of atoms in the A_g vibrational modes with frequencies of 793 cm^{-1} (a) and 484 cm^{-1} (b). Dark gray, gray, and light gray spheres denote vanadium, oxygen, and lithium atoms, respectively.

Li atoms. The spectra of the γ-LiV_2O_5 and γ'-V_2O_5 structures are compared in Figure 4, and one sees that the spectra are different, especially in the low-frequency region. In the region above 400 cm^{-1}, comparison of the spectra reveals the following principal differences:

1. The high-frequency peaks at 1000 cm^{-1} in the spectrum of γ-LiV_2O_5 are downward shifted as compared to positions of their counterparts in the spectrum of γ'-V_2O_5.
2. A wide intense peak at 737 cm^{-1} in the spectrum of γ-LiV_2O_5 substitutes for a complex spectral feature observed in the spectrum of γ'-V_2O_5 at around 700 cm^{-1}.
3. A new weak peak at ca. 650 cm^{-1} appears in the spectrum of γ-LiV_2O_5, whereas the peak at 600 cm^{-1} in the spectrum of γ'-V_2O_5 disappears.
4. A new intense and wide peak appears in the spectrum of γ-LiV_2O_5 at 462 cm^{-1}.

The origins of these differences can be understood by comparing the assignment of the Raman peaks in Table 4 with that given in ref 17 for the Raman spectrum of γ'-V_2O_5 and by making use of the structural data in Table 2.

The above-mentioned downward shift of the two high-frequency peaks 1a and 1b in the spectrum of the lithiated structure is clearly caused by the lengthening of the V−O1 bonds upon interaction of the O1 atoms with Li atoms. According to both the experimental and computational data (Table 2), the length of the V−O1 bonds increases by ca. 0.03−0.05 Å, and the use of the empirical correlation of V−O bond-stretching frequency versus V−O bond length[36] results in a frequency shift of 60−100 cm^{-1} for the V−O1 bond-stretching vibrations. This estimation is slightly larger than the shift of 40−60 cm^{-1} observed in the experimental spectra and obtained in the calculations. The discrepancy can be explained as a result of the interaction of O1 atoms with lithiums that raises the frequency of the V−O1 modes. The calculations show that the peak 1a can be assigned to the A_g mode with antiphase stretching vibrations of the Va−O1b and Vb−O1b bonds, whereas peak 1b is due to such inphase vibrations.

The other distinctions between the spectra of the two materials have the same origin. The large difference in the length of the Va−O3 and Vb−O3 bonds in the γ-LiV_2O_5 structure (cf. Table 2) leads to a marked disparity of the Va−O3 and Vb−O3 bond-stretching force constants. As a result, the V−O stretching vibrations in the Va−O3−Vb bridges cannot be anymore represented as the antisymmetric ν_{as} and symmetric ν_s combinations, as was done for the γ'-V_2O_5 lattice.[17] The above-mentioned disappearance of the peak at 600 cm^{-1} in the spectrum of γ'-V_2O_5, which has been assigned to the ν_s Va−O3−Vb mode,[17] is just the consequence of such structural change. The peak at 600 cm^{-1} can therefore be used as a fingerprint of quasi-symmetric Va−O3−Vb bridges inherent in the γ'-V_2O_5 structure. Instead of the ν_{as} and ν_s combinations, we should now consider ν(Va−O3) and ν(Vb−O3) bond-stretching vibrations in the γ-LiV_2O_5 structure. According to the present DFT calculations, the frequencies of the corresponding A_g modes are 793 and 484 cm^{-1}, respectively, and atomic displacements in these modes are shown in Figure 6. The former mode is a pure Va−O3 stretching vibration, whereas the latter also involves V−O ladder step vibrations.

The wide and intense peak at 737 cm^{-1} in the Raman spectrum of the γ-LiV_2O_5 sample can therefore be related to the Va−O3 bond-stretching mode (Figure 6a). This peak also covers signal due to the B_{1g}/B_{3g} twin-mode computed at 736 cm^{-1}. According to the DFT calculations, the mode comes from the antisymmetric combination ν_{as}(Va−O2a−Va) of Va−O2a stretching vibrations localized in the V_2O_5 chains. The analogous ν_{as}(Vb−O2b−Vb) mode has the theoretical frequency of 628 cm^{-1}, and it is the origin of peak 3b at 646 cm^{-1} in the spectrum of γ-LiV_2O_5. It is worthy of note that peaks due to these two ν_{as}(V−O2−V) modes have been observed at 737 and 646 cm^{-1} in the single-crystal Raman spectra in the *ab* and *bc* polarizations.[34] In the spectrum of the γ'-V_2O_5 structure the ν_{as}(Va−O2a−Va) and ν_{as}(Vb−O2b−Vb) modes are at 721 and 694 cm^{-1}, respectively.[17] The frequency difference between these modes in the two structures is due to the change of V−O bond lengths upon lithium intercalation (Table 2).

Another marked distinction between the spectra of the γ'-V_2O_5 and γ-LiV_2O_5 structures is the presence of an intense peak at 462 cm^{-1} in the spectrum of the lithiated structure (Figure 4). This feature can be related to peak at 456 cm^{-1} observed in

DOI: 10.1021/acs.jpcc.5b05540
J. Phys. Chem. C 2015, 119, 20801−20809

single-crystal spectra measured in the *bb* and *cc* polarization settings.[34] Consequently, the peak is due to a mode of the A_g symmetry, and we attribute it to the ν(Vb−O3) mode computed at 484 cm^{-1} with the atomic displacements in the mode shown in Figure 6b.

The proposed attribution of the peaks at 737 and 462 cm^{-1} is corroborated by the calculated Raman spectra shown in Figure 7. One sees that the peaks due to the ν(Va−O3) and ν(Vb−O3) modes have strong Raman intensities in line with the experimental spectrum in the corresponding regions. Interestingly, the parent ν_{as}(Va−O3−Vb) and ν_s(Va−O3−Vb) modes yield much less intense signals (peaks 2 and 4 in the spectrum of γ'-V_2O_5 in Figure 4).

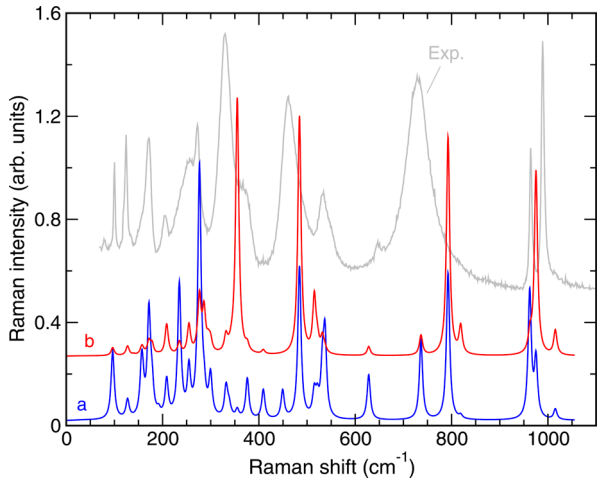

Figure 7. Experimental and calculated (a, b) Raman spectra of γ-LiV_2O_5. Theoretical spectra a and b were computed for ω = 241.8 THz and ω = 604.5 THz (1 and 2.5 eV), respectively (see Computational Details).

The spectral region from 500 to 550 cm^{-1} also contains Raman peaks related to the vibrations localized in the V−O ladder steps that are shown in Figure 2 by dashed lines. According to the DFT calculations, the two modes corresponding to the $(Va{-}O2a)_{LS}$ and $(Vb{-}O2b)_{LS}$ bond-stretching vibrations have close frequencies of 532 and 515 cm^{-1}, respectively. These modes give rise to peak 5 in the γ-LiV_2O_5 spectrum (Figure 4). Frequencies of these modes in the γ'-V_2O_5 and γ-LiV_2O_5 structures are very close to each other as the length of the ladder steps remains essentially unchanged upon Li intercalation. It should be mentioned that the two components of the doublet have been observed at 550 and 528 cm^{-1} in the polarized Raman spectra recorded at low temperature (cf. Figure 3a in ref 34), and their assignment is in line with that proposed in the reference.

The frequency values of the V−O stretching modes with nonbridging oxygen atom (V−O1, V−O2 ladder steps) correlate well with the values of bond lengths listed in Table 2, and this correlation is in good agreement with the empirical relationship found in ref 36. It is noteworthy that the frequencies of two modes of Va−O3−Vb bridges follow the same dependence that is in line with the above discussion. On the other hand, V−O2−V bridges are quasi-symmetric with a large V−O2−V angle (130−140°) and, thus, the effective force constant in the ν_{as}(Va−O2a−Va) and the ν_{as}(Vb−O2b−Vb) modes is approximately 2 times the corresponding V−O2 bond-stretching force constant. Consequently, the frequencies of these modes deviate from the relationship of ref 36 but still correlate with the length of the Va−O2a and Vb−O2b bonds.

Raman-active modes involving large-amplitude vibrations of Li atoms were computed in the region from 450 to 230 cm^{-1}, and Li modes above 400 cm^{-1} appear in a "transparency window", where no Raman-active modes are present in the spectrum of the γ'-V_2O_5 structure. Unfortunately, in the lithiated structure the corresponding Raman signal cannot be observed because of the intense ν(Vb−O3) peak, whereas vibrations of Li atoms in other modes are strongly coupled with low-frequency vibrations of vanadate lattice and the corresponding Raman signals lack their identity.

CONCLUSIONS

The structure, electronic states, and Raman spectrum of γ-LiV_2O_5 were studied with a combined use of experimental and computational techniques. The DFT calculations were found to correctly reproduce the experimental structural data of the γ-LiV_2O_5 lattice.

In agreement with the previous studies[12,13,16] the electronic structure of the material reveals the presence of gap states accepting the 2*s* electrons of the Li atoms. Analysis of the wave functions of the states indicates that they mainly consist of the 3*d*(Vb) contributions and that the four electrons occupied these states are aligned in ferromagnetic order. The computation of charge distribution shows that the transferred electron is mostly spread over the O1b−Vb−O2b entity of the vanadate framework. The amount of negative charge received by the Vb atom is in good agreement with the experimental value estimated by UV photoelectron spectroscopy.[16]

Comparison of the experimental and calculated Raman spectra of γ-LiV_2O_5 and comparison of these results with the recently studied vibrational dynamics of γ'-V_2O_5 structure[17] allowed us to propose a reliable assignment for all prominent features in the spectral region above 400 cm^{-1}. The differences in the spectra of the two materials were related to the structural modifications induced by the Li atoms insertion into the interlayer space. The notable downward shift of Raman peaks attributed to the ν(Va−O1b) and ν(Vb−O1a) modes is due to the lengthening of the vanadyl V−O1 bonds in the lithiated structure. The Li intercalation also causes an increase of asymmetry of the Va−O3−Vb bridges that leads to the transformation of the asymmetric ν_{as} and symmetric ν_s Va−O3−Vb vibrations into ν(Va−O3) and ν(Vb−O3) bond-stretching vibrations. The transformation is accompanied by significant change of the Raman spectrum in which new intense Raman peaks at 737 and 462 cm^{-1} resulting from the ν(Va−O3) and ν(Vb−O3) vibrational modes appear. The proposed attribution is corroborated by the computation of the Raman spectrum including the mode intensities. The outcome of the study allows the identification of spectral manifestation related to specific structural changes in the V_2O_5 framework.

AUTHOR INFORMATION

Corresponding Author

*(M.B.S.) E-mail: smirnomb@rambler.ru.

Notes

The authors declare no competing financial interest.

ACKNOWLEDGMENTS

This work was supported by the international collaboration program between the Centre National de la Recherche

DOI: 10.1021/acs.jpcc.5b05540
J. Phys. Chem. C 2015, 119, 20801−20809

Scientifique (CNRS) of France and the Russian Foundation for Basic Research (RFBR), LIBASTRAM CNRS Project 6094, and RFBR Grant 13-03-91052.

REFERENCES

(1) Whittingham, M. S. Lithium Batteries and Cathode Materials. *Chem. Rev.* **2004**, *104*, 4271−4301.
(2) Galy, J. Vanadium Pentoxide and Vanadium Oxide Bronzes − Structural Chemistry of Single (S) and Double (D) Layer $M_xV_2O_5$ Phases. *J. Solid State Chem.* **1992**, *100*, 229−245.
(3) Murphy, D. W.; Christian, P. A.; DiSalvo, F. J.; Waszczak, J. V. Lithium Incorporation by Vanadium Pentoxide. *Inorg. Chem.* **1979**, *18*, 2800−2803.
(4) Dickens, P. G.; French, S. J.; Hight, A. T.; Pye, M. F. Phase Relationships in the Ambient Temperature $Li_xV_2O_5$ System ($0.1 < x < 1.0$). *Mater. Res. Bull.* **1979**, *14*, 1295.
(5) Galy, J.; Darriet, J.; Hagenmuller, P. $Li_xV_2O_5$ Bronzes − Structure of β'-Phase and Refinement of γ-Phase Structure. *Rev. Chim. Miner.* **1971**, *8*, 509−511.
(6) Galy, J.; Hardy, A. Structure Cristalline du Bronze de Vanadium-Lithium LiV_2O_5. *Acta Crystallogr.* **1965**, *19*, 432−435.
(7) Delmas, C.; Cognac-Auradou, H.; Cocciantelli, J. M.; Menetrier, M.; Doumerc, J. P. The $Li_xV_2O_5$ System: An Overview of the Structure Modifications Induced by the Lithium Intercalation. *Solid State Ionics* **1994**, *69*, 257−264.
(8) Cocciantelli, J. M.; Doumerc, J. P.; Pouchard, M.; Broussely, M.; Labat, J. Crystal Chemistry of Electrochemically Inserted $Li_xV_2O_5$. *J. Power Sources* **1991**, *34*, 103−111.
(9) Cocciantelli, J. M.; Gravereau, P.; Doumerc, J. P.; Pouchard, M.; Hagenmuller, P. On the Preparation and Characterization of a New Polymorph of V_2O_5. *J. Solid State Chem.* **1991**, *93*, 497−502.
(10) Willinger, M.; Pinna, N.; Su, D. S.; Schlogl, R. Geometric and Electronic Structure of γ-V_2O_5: Comparison Between α-V_2O_5 and γ-V_2O_5. *Phys. Rev. B: Condens. Matter Mater. Phys.* **2004**, *69*, 155114.
(11) Ganduglia-Pirovano, M. V.; Sauer, J. Reduction of the (001) Surface of γ-V_2O_5 Compared to α-V_2O_5. *J. Phys. Chem. B* **2005**, *109*, 374−380.
(12) Valentí, R.; Saha-Dasgupta, T.; Alvarez, J. V.; Požgajčić, K.; Gros, C. Modeling the Electronic Behavior of γ-LiV_2O_5: A Microscopic Study. *Phys. Rev. Lett.* **2001**, *86*, 5381−5384.
(13) Scanlon, D. O.; Walsh, A.; Morgan, B. J.; Watson, G. W. An ab initio Study of Reduction of V_2O_5 through the Formation of Oxygen Vacancies and Li Intercalation. *J. Phys. Chem. C* **2008**, *112*, 9903−9911.
(14) Weber, W. H., Merlin, R., Eds. *Raman Scattering in Materials Science*; Springer: Berlin, Germany, 2000.
(15) Li, Z.; Wu, Q. H. Electronic Structures of $M_xV_2O_5$ (x = 0.5 and 1): A Theoretical Study. *ChemPhysChem* **2008**, *9*, 300−304.
(16) Wu, Q.-H.; Thißen, A.; Jaegermann, W. Photoelectron Spectroscopic Study of Li Intercalation into V_2O_5 Thin Films. *Surf. Sci.* **2005**, *578*, 203−212.
(17) Baddour-Hadjean, R.; Smirnov, M. B.; Kazimirov, V. Y.; Smirnov, K. S.; Pereira-Ramos, J. P. The Raman Spectrum of the γ'-V_2O_5 Polymorph: A Combined Experimental and DFT Study. *J. Raman Spectrosc.* **2015**, *46*, 406−412.
(18) Dai, J. X.; Li, S. F. Y.; Gao, Z. Q.; Siow, K. S. N. Novel Method for Synthesis of γ-Lithium Vanadium Oxide as Cathode Materials in Lithium Ion Batteries. *Chem. Mater.* **1999**, *11*, 3086−3090.
(19) Larson, A.; Von Dreele, R. *General Structure Analysis System (GSAS)*; Los Alamos National Laboratory: Los Alamos, NM, USA, 2004
(20) Toby, B. EXPGUI, A Graphical User Interface for GSAS. *J. Appl. Crystallogr.* **2001**, *34*, 210−213.
(21) Kresse, G.; Hafner, J. *Ab Initio* Molecular-Dynamics Simulation of the Liquid-Metal-Amorphous-Semiconductor Transition in Germanium. *Phys. Rev. B: Condens. Matter Mater. Phys.* **1994**, *49*, 14251−14269.
(22) Kresse, G.; Furthmüller, J. Efficiency of Ab-Initio Total Energy Calculations for Metals and Semiconductors Using a Plane-Wave Basis Set. *Comput. Mater. Sci.* **1996**, *6*, 15−50.
(23) Perdew, J. P.; Burke, K.; Ernzerhof, M. Generalized Gradient Approximation Made Simple. *Phys. Rev. Lett.* **1996**, *77*, 3865−3868.
(24) Blöchl, P. E. Projector Augmented-Wave Method. *Phys. Rev. B: Condens. Matter Mater. Phys.* **1994**, *50*, 17953−17979.
(25) Kresse, G.; Joubert, D. From Ultrasoft Pseudopotentials to the Projector Augmented-Wave Method. *Phys. Rev. B: Condens. Matter Mater. Phys.* **1999**, *59*, 1758−1775.
(26) Dudarev, S. L.; Botton, G. A.; Savrasov, S. Y.; Humphreys, C. J.; Sutton, A. P. Electron-Energy-Loss Spectra and the Structural Stability of Nickel Oxide: An LSDA+U Study. *Phys. Rev. B: Condens. Matter Mater. Phys.* **1998**, *57*, 1505−1509.
(27) Londero, E.; Schröder, E. Vanadium Pentoxide (V_2O_5): A van der Waals Density Functional Study. *Comput. Phys. Commun.* **2011**, *182*, 1805−1809.
(28) Carrasco, J. Role of van der Waals Forces in Thermodynamics and Kinetics of Layered Transition Metal Oxide Electrodes: Alkali and Alkaline-Earth Ion Insertion into V_2O_5. *J. Phys. Chem. C* **2014**, *118*, 19599−19607.
(29) Grimme, S. Semiempirical GGA-Type Density Functional Constructed with a Long-Range Dispersion Correction. *J. Comput. Chem.* **2006**, *27*, 1787−1799.
(30) Murnaghan, F. D. The Compressibility of Media under Extreme Pressures. *Proc. Natl. Acad. Sci. U. S. A.* **1944**, *30*, 244−247.
(31) Monkhorst, H. J.; Pack, J. D. Special Points for Brillouin-Zone Integrations. *Phys. Rev. B* **1976**, *13*, 5188−5192.
(32) Gajdoš, M.; Hummer, K.; Kresse, G.; Furthmüller, J.; Bechstedt, F. Linear Optical Properties in the Projector-Augmented Wave Methodology. *Phys. Rev. B: Condens. Matter Mater. Phys.* **2006**, *73*, 045112.
(33) Bader, R. F. W. *Atoms in Molecules − A Quantum Theory*; Oxford University Press: Oxford, UK, 1990.
(34) Popović, Z.; Gajić, R.; Konstantinović, M. J.; Provoost, R.; Moshchalkov, V. V.; Vasil'ev, A. N.; Isobe, M.; Ueda, Y. Infrared and Raman Spectra of LiV_2O_5 Single Crystals. *Phys. Rev. B: Condens. Matter Mater. Phys.* **2000**, *61*, 11454.
(35) Baddour-Hadjean, R.; Rackelboom, E.; Pereira-Ramos, J. P. New Structural Characterization of the $Li_xV_2O_5$ System Provided by Raman Spectroscopy. *Chem. Mater.* **2006**, *18*, 3548−3556.
(36) Hardcastle, F.; Wachs, I. Determination of Vanadium-Oxygen Bond Distances and Bond Orders by Raman Spectroscopy. *J. Phys. Chem.* **1991**, *95*, 5031−5041.

DOI: 10.1021/acs.jpcc.5b05540
J. Phys. Chem. C 2015, 119, 20801−20809